3rd International Workshop on PIV'99-Santa Barbara
Fess Parker's Double Tree Resort, Santa Barbara, CA, USA
September 16-18, 1999

Panoramic-PIV system and its application to tandem oil fences

D. H. Doh, B. S. Hyun, K. H. Bang, S. D. Hong, T. S. Baek, T. Saga, T. Kobayashi

Abstract A Panoramic PIV system is developed using three commercial CCD cameras of which pixel resolution is 768 x 494. An image composition process is made to make Panoramic images obtained by the respective CCD camera. The velocity vectors are obtained by the grey level cross-correlation method. An experimental investigation into the vortex-to-vortex interaction of the flow between two fences set in tandem is made by using the constructed Panoramic PIV system. Further, the velocity spectra of the oscillating flow behind the downstream oil fence are also obtained to predict the characteristics of the tip vortex shedding. This system is applicable to a wide range of measurement in which high spatial resolution is required.

List of symbols

C_{fg}	cross-correlation coefficient
f_i	grey level of first image
g_i	grey level of second image
$\overline{fi}$	average grey level in cross-correlation area of first image
$\overline{gi}$	average grey level in cross-correlation area of second image
g	gravitational acceleration
n^2	pixel number in cross-correlation area
U	mean velocity of mainstream
Δ	density ratio
ρ_w	density of water
ρ_o	density of oil

D. H. Doh, K. H. Bang, S. D. Hong, T. S. Baek
Division of Mechanical Systems Engineering
Korea Maritime University
1 Dongsam-dong, Youngdo-ku, 606-791, Korea

B. S. Hyun,
Division of Naval Architecture and Ocean Engineering
Korea Maritime University
1 Dongsam-dong, Youngdo-ku, 606-791, Korea

T. Saga, T. Kobayashi
Institute of Industrial Science, Tokyo University
7-22-1, Roppongi, Minato-ku, tokyo 106, Japan

1 Introduction

An oil fence is one of the important devices for the containment and recovery of spilt oil in a sea. In spite of its important roles in oil-spill accidents, the proper function of an oil fence can be anticipated in limited situations only due to the existence of surface currents and ocean waves. Generally, the single oil fence loses its containment capability if the sea current is over 0.3 m/sec due to the interaction among parameters such as density difference between oil and water, gravity, current speed and surface tensions (Song et al. 1998). To overcome this critical limits in the effectiveness of a single fence, the idea of tandem fences was proposed by Delvigne (1987) and Lo (1996). The fences can be deployed in tandem to retrap the leaked oil in the shelter formed between the two fences. This shelter of relatively low shear rate on oil-water interface can effectively retain the leaked oil far beyond the critical current velocity at which a single fence fails to contain the oil layer(Lee & Kang 1997 1998).

Two key-issues in using the tandem fences are (1) to trap safely the spilt oil droplets escaped over the first fence between the tandem fence, and (2) to maintain the trapped oil not to leak out of the tandem fence. While the first issue can be easily solved by making the distance between fences wider, an optimal distance should be determined by considering the second issue.

In the present study, the flow field between two fences was visualized and analyzed using PIV technique(Adrian 1991), microscopically. Experiments were made in a single fluid (water) without oil layer, and then an oil layer on it.

In order to investigate the flow without oil layer between the oil fences microscopically, a new Panoramic PIV system is constructed, and the characteristics of the travelling wavy motions and the complex small scale vortical flow structures are quantified. Kang and Lee (1998) numerically confirmed that the appearance of the travelling wavy motion was mainly due to small vortices in the tandem fence.

In Panoramic PIV system, three CCD cameras are used in coincidence mode, and a new image composition technique is applied to combine 3 sets of images acquired by three different cameras. Using the constructed Panoramic PIV system, the dynamic behavior of the oil-water interfaces in the tandem is discussed in more detail.

2 Investigation for the flow in tandem fence by Panoramic PIV

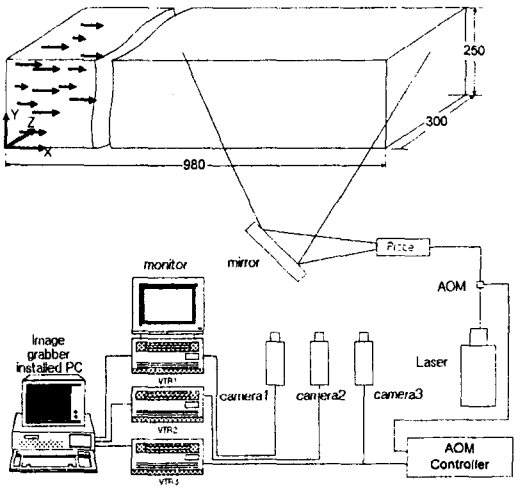

Fig. 1 Panoramic PIV system for microscopic investigation for the flow in the tandem oil fence

Since the analysis made by the conventional PIV system using one camera is not precise enough to capture the movements of the small scaled vortices, a new PIV system called "Panoramic PIV" is introduced to quantitatively investigate the mechanism of the vortex-to-vortex interactions of the flow between the two tandem plates.

Experiments have been made in a single fluid (water) without oil layer on it at first and then with an oil layer using the newly constructed Panoramic PIV system..

2.1 Experimental apparatus and procedures

Figure 1 shows the constructed Panoramic PIV system for a microscopic investigation for the flow generated by the tandem plates. The tandem plates are set in a circulating water channel whose test section has a dimension of 1m long x 0.3m wide x 0.25m deep. The shape of the tandem fence is a flat plate as shown in Fig. 2. The thickness of the plate is 4mm and its angle, θ, is set to zero. The draft of the plate, d, is 4cm. For panoramic measurement, three cameras (Sony, SSC-M370) were set in parallel in order to capture the closer and wider view against the same circulating water channel used for the macroscopic experiment and synchronized for coincident measurement for the whole flow field in close-up mode. The light source of Ar-Ion laser (500mW) is controlled by AOM (Acousto-Optical Modulator) system (Kobayashi et al. 1991) and passes through a LLS (Laser Light Sheet) probe. For visualization, the laser light sheet is reflected by a mirror and emitted into the flow field in the middle of test section to visualize the desired area only. AOM system is used to enhance the dynamic range of velocity tracking

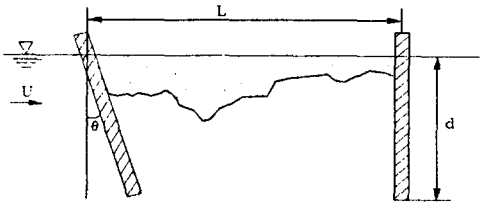

Fig. 2 Tandem oil fences

since this system is able to control the cut-off time of the light source so that the illumination time for the particles is to be controlled. The images captured by the three cameras are recorded onto three video tape recorders, VTR1 (Panasonic, AG-7350), VTR2 (Sony, SLV-RS1), and VTR3 (SLV-595HF), or an image processor (Ditect, DT-64) installed on a host computer (Pentium 300MHz).

In order to reconstruct a Panoramic image, each image captured by those three cameras is composed altogether. A calibration process should be carefully made to acquire the composition of correct image for three images captured by the three cameras.

Figures 3(a), (b), and (c) show the images of a calibration plate on which mesh lines are plotted with a fixed interval of 10mm. Using the information of relative position of the mesh line on each image, a panoramic image is constructed for three different images which have been taken at the coincidence mode.

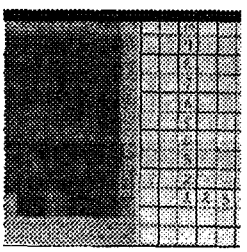

(a) Image of camera 1

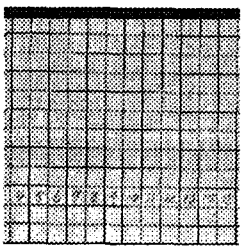

(b) Image of camera 2

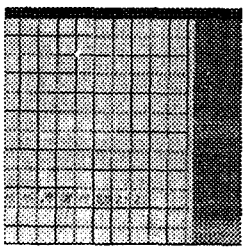

(c) Image of camera 3

Fig. 3 Images of the calibration plate

Figure 4 shows the composed image for the calibration plate viewed by three cameras. Completing the calibration

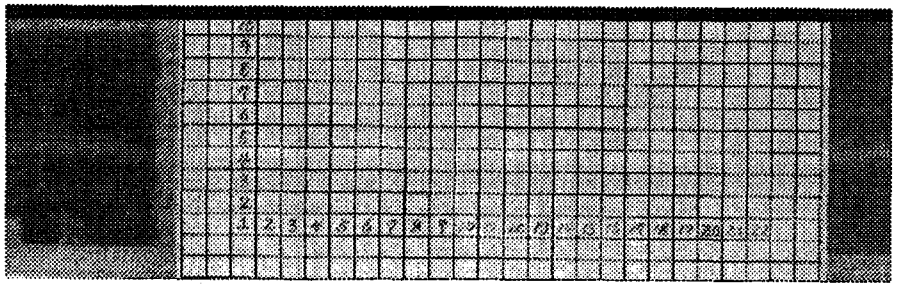

Fig. 4 Composed image from the images from three cameras

works, tracer particles (Nylon 12, diameter = 100μm, specific gravity = 1.02) are injected into the water flowing with 0.33m/sec in the circulating water channel for visualization. The visualized images are then recorded onto the same image grabber and VTR's mentioned above. Grabbed images are digitized into 256 grey levels and are separated into two fields, namely "odd" and "even" fields, in order to construct two images taken with the time interval, 19msec, as shown in Fig. 5 which shows the time relation between the AOM pulse signal and the NTSC video signal. The pulse signal for AOM is activated twice; the one is in the odd field of a frame and the other is in the even field of the same frame with the same pattern. Therefore, two particle images are seen for one particle on one frame.

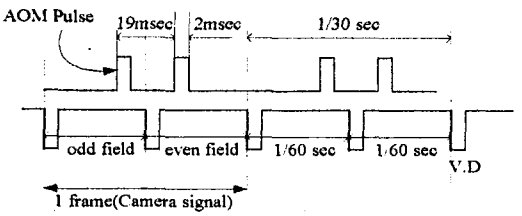

Fig. 5 Relations between NTSC(camera signal) and AOM signals

2.2
Velocity vector acquisition

Velocity vectors are obtained based on the grey-level cross-correlation method (Kimura et. al., 1986; Utami and Blackwelder 1991) from the grey level field images. This is based upon the "two-fields cross-correlation method" in which the coordinate indicating the maximum coefficient is assumed to be a vector terminal point. The searching area is a circle drawn with the radius whose length is maximum allowable distance between the grid point of the first image and the terminal point of the second image. The grey levels of the whole pixels in the correlation area of the first and second images are cross-correlated within the searching area. Equation (1) is the formula employed to calculate the cross-correlation coefficients. The magnitude of the velocity vectors are obtained by calculating the correlation coefficients for those two field images and

$$c_{fg} = \frac{\sum_{i=1}^{n^2}(f_i - \overline{f_i})(g_i - \overline{g_i})}{\sqrt{\sum_{i=1}^{n^2}(f_i - \overline{f_i})^2 \sum_{i=1}^{n^2}(g_i - \overline{g_i})^2}} \quad (1)$$

then dividing it with the time inter- val of 19 msec. Here, f_i and g_i denote the grey levels of the each pixel within the correlation region on the 1st and 2nd frames, respectively, and "-" over these letters indicates an average value of the grey levels of the pixels within the correlation region. And n^2 means the number pixels in the correlation area. The terminal point of the velocity vector is decided as a point on which the calculated coefficient is the maximum value in the searching area. Since the velocity vectors are obtained based on pixel resolution, a positional uncertainty is at least ± 1 pixel within the results. The sub-pixel resolution method (Utami and Blackwelder 1991) was adopted in order to enhance the accuracy of velocity measurement. Furthermore, an error vector elimination method (Hojo and Takashima, 1995) based on the continuous flow condition was adopted since there might be some erroneous vectors depending on the size of correlation area and the distance of the searching area.

2.3
Results and discussions on single fluid(water) experiment

Figure 6 shows an instantaneous velocity vector field obtained by the image constructed with Panoramic PIV system when L/d is 8 and the mean velocity of main stream is 0.33m/sec.

From the figure it can be said that small vortex structures are seen in more detail, which has not been done with conventional PIV methods. And it can be seen that the tip vortex created at the tip of the first tandem plate is convected toward downstream with the large travelling wavy structure. It seems that this wavy structure is originated from the tip vortex created at the tip of the upstream plate. This counter-clockwise vortex is convected to downstream until hitting the front wall of the second tandem fence, and produces an induced velocity component toward the free surface in front of the second wall. This induced velocity component raises the height of

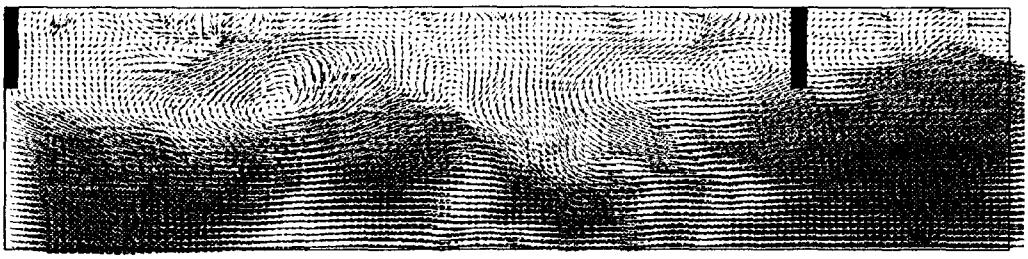

Fig. 6 Instantaneous velocity vector distribution obtained by Panoramic PIV

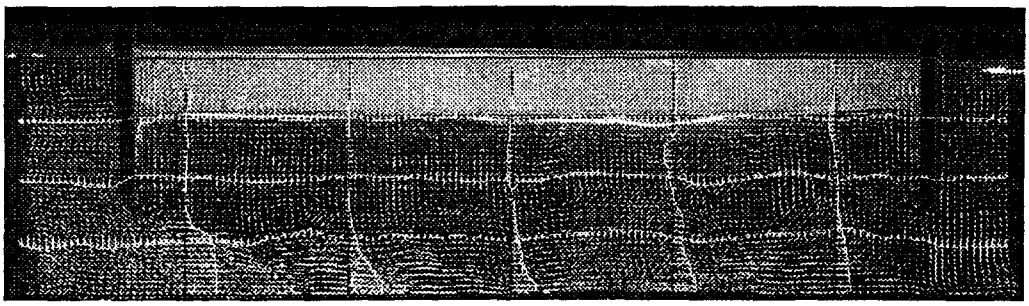

Fig. 7 Instantaneous velocity vector distribution of the whole tandem flow field (U = 0.14 m/sec)

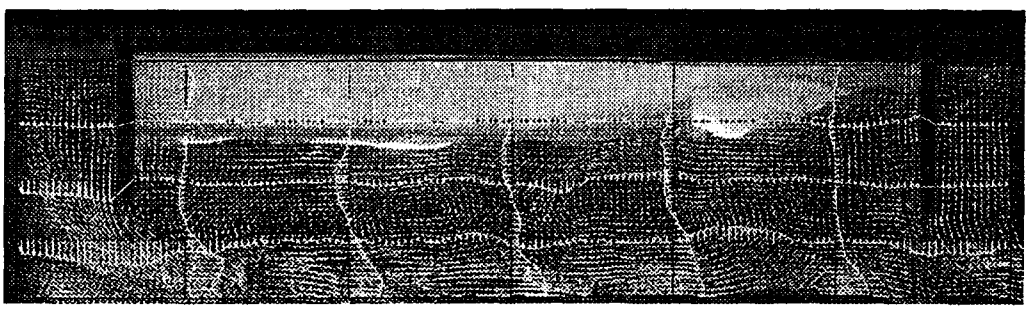

Fig. 8 Instantaneous velocity vector distribution of the whole tandem flow field (U = 0.22 m/sec)

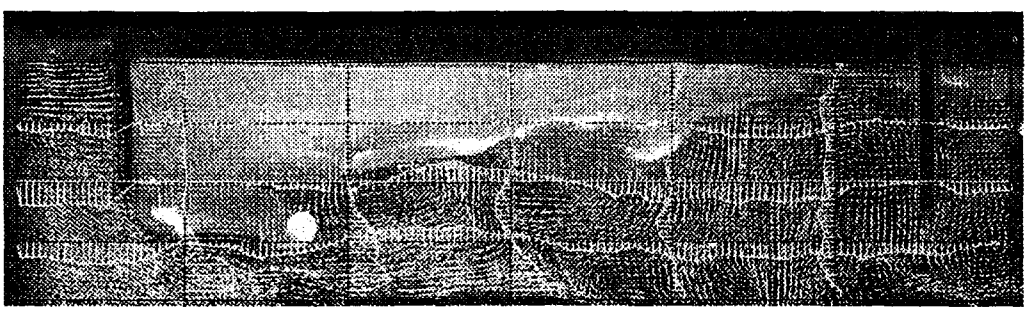

Fig. 9 Instantaneous velocity vector distribution of the whole tandem flow field (U = 0.28 m/sec)

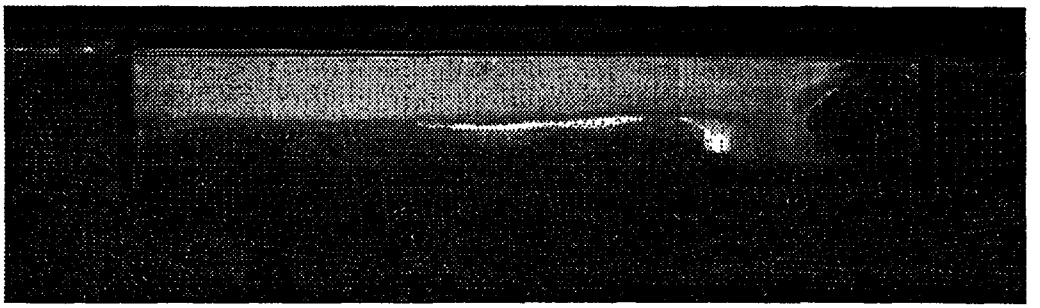

Fig. 10 Instantaneous velocity vector distribution of the whole tandem flow field (U = 0.22 m/sec)

surface water near the second wall and makes the water surface unstable. This phenomenon may also occur in practical flow fields at sea. Since the tip vortices are consecutively convected to downstream, the water surface becomes more unstable and undulated. This free surface flow will again affect the vortical flow field below water surface, which implies that the oil layer would move back and forth owing to the periodic motion of the driving fluid (water) if there is an oil layer on the water. When the total shear forces imposed to the oil layer from the water are large enough to push the trapped oil lump toward upstream, the volumetric increase of oil at the upstream tandem plate occurs and eventually causes the trapped oil separated by the tip vortices.

2.4
Results and discussions on oil-water experiment

In order to quantitatively investigate the flow characteristics in the tandem, a lump of soybean oil (1,400 cc, specific gravity = 0.91, 55 cst at 25℃) is injected into the water and an experiment is carried out in the same way. The densimetric Froude number were in three conditions, Frd = 0.8 (U=0.14m/sec), Frd = 1.2 (U=0.22m/sec), Frd = 1.5 (U=0.28m/sec), where $Frd = U/\sqrt{\Delta gd}$, U is the mean velocity of mainstream, g is gravitational acceleration, and $\Delta=(\rho_w - \rho_o)/\rho_w$,. Here, ρ_w is water density and ρ_o is oil density. The distance between the two tandem plates, L/d, was maintained at 7.

Figures 7, 8, and 9 show the panoramic instantaneous velocity distribution at each Frd number. The tip vortices are clearly seen and convected to downstream with the undulated structure. However, these undulations are not so conspicuous compared to the cases shown in the previous section without oil layer. The oil layer is more stable at smaller Frd numbers. The shape of oil-water interface appears very complicated as seen in Figs. 7, 8, 9, and 10, and these kinds of interface profile have been consistent for most of experimental results. Contrarily the free surface flow on oil-air interface is quite calm and stable compared to that on water-air interface without oil layer, which exhibits violent movement on free surface.

As in the case of single fluid in the previous section, the tip vortices are also consecutively convected to downstream and are reflected at the second plate toward upstream making various vortical structures. The whole flow field shows two conspicious parts. One is the outer flow at which the main current exists and the velocity is relatively higher than at any other place. The other is the inner flow between the two plates, at which the velocity is lower. From Fig. 7, it can be said that the shear stress of the boundaries between the water and the oil layer is not so big enough to make the inner flow field unstable. However, a relatively large vortex rotating counterclockwise near the front side of the second plate at downstream produces a reverse shear force making the oil layer move a little toward upstream. In the case of Fig. 8, the flow characteristics are largely different from those in Fig. 7.

The strength of the vortices rotating counterclockwise in the low velocity zone became stronger and a recirculating zone appeared making the reverse shear forces more stronger. This eventually makes the oil layer move toward upstream (left side). The reflected vortices at the front side of the second plates of downstream (right side) produces a pressure field which causes the oil layer unstable and undulated. This unstable phenomenon also appears intermittently at other boundaries enhancing the instability of the oil-water interface of the whole inner flow field.

Figure 10 shows one of the conspicious unstable phenomenon at the downstream at the same Frd number as that of Fig. 8. An onset of oil breaking is visible. The oil is just about to plunge into the water side owing to the pressure increase at that place. If this onset plunges onto the place where either high pressure gradient or high frictional stress exists by the main current, the oil droplets from the apex of elongated oil lump are escaped into water side, and then the oil entrainment failure occurs.

The shorter the generation period of the tip vortex at the tip of the first plate is, which is due to the increase of mainstream velocity, the bigger the unsteady force from the reflected vortices is. This eventually makes the oil layer move toward upstream and results in the increase of the oil thickness at the rear part of first tandem plate where the thickness of oil layer is limited by the draft of the plate. If this unsteady forces become more stronger owing to the increase of mainstream velocity, the volume increase of oil per unit hour at the rear part of the first

plate makes the oil thickness exceed the draft of the plate, and this eventually makes some parts of the oil lump meet with the tip vortices, and then oil entrainment failure occurs with a similar manner as the entrainment failure of the onset oil lump near the front part of the second tandem plate.

In summary of experimentally observed results, there are two distinct locations of critical oil failure between the tandem plates. One is at the rear part of the upstream tandem plate where strong tip vortices are created periodically. This is the consequence of reverse flow generated just under the oil-water interface induced by tip vortices, demonstrating the role of frictional force acting on the interface. The other is in front of the second fence where the convected tip vortex is trapped and high pressure region is produced as a result of the collision of convected vortex against the second fence. The failure of oil droplets occurs when the elongated oil lump no longer resists against the high pressures imposed from both sides of that oil lump, demonstrating the role of pressure force. This makes the "entrainment failure" of oil from the apex of elongated oil lump, the phenomenon similar to the typical failure mode occurred near the headwave of oil slick contained by a single fence. (Song et al. 1998)

3 Conclusions

The flow behaviour in the tandem plates has been investigated microscopically. The dynamic behavior of the whole flow field without and with oil-water interface in the tandem has been investigated more precisely using a newly-developed Panoramic PIV technique. The important experimental results are summarized as follow;

The oil layer tends to move toward upstream owing to the existence of the shear force acting on oil-water interface caused by vortical structures under the oil layer. It results in the increase of the oil thickness at the rear part of first tandem fence where the thickness of oil layer is limited by the draft of fence.

It has been experimentally observed that there are two locations where the critical oil failure exists between the tandem plates. One is at the rear part of the upstream tandem plate where strong tip vortices are created periodically. The other is in front of the second fence where the convected tip vortex is trapped and high pressure region is produced as a result of the collision of convected vortex against the second fence. The failure of oil droplets occurs when the elongated oil lump no longer resists against the high pressures imposed from both sides of that oil lump. This makes the "entrainment failure" of oil from the apex of elongated oil lump.

Finally it has been found that the newly developed Panoramic PIV system could be successfully applied to the analysis of small eddy structures and is expected to be utilized for elucidating the mechanisms of various kinds of small scale vortex-to-vortex interactions.

References

Adrian RJ (1991) Particle-imaging techniques for experimental fluid mechanics. Ann. Rev. Fluid Mech., 23: 261-304

Buchhave P (1992) Particle image velocimetry-status and trends. Exp. Thermal and Fluid Sci., 5: 586-604

Delvigne GAS (1987) Laboratory experiments on oil spill protection of a water intake. In oil in fresh water: Chemistry, Biology, Countermeasure Technology, (Eds. J. H. Vandermeulen, and S. E. Hrudey). Pergamon Press: 446-458

Hojo K; Takashima H (1995) Detection of erroneous velocity vectors obtained in PIV. J. of Visualization Society of Japan, 15-2: 177-180

Kang KH; Lee CM (1998) Behavior of oil-water interface between tandem fences. Proc. of the Spring Meeting of the Krrean Society for Marine Environmental Engineering: 221-226

Kimura I; Takamori T; Inoue T (1986) Image Processing Instrumentation of flow by using correlation technique. Flow Visualization, 6-22: 105-108

Kobayashi T; Saga T; Haeno T; Tsuda N (1991) Development of a real-time velocimetry measurement system for high reynolds fluid flow using a digital image processing design. ASME FED, 128: 1220-1227

Lee CM; Kang KH (1998) Analysis of containment capability of oil fence in currents and waves. J. of Korean Soc. for Marine Environmental Eng., 1-1: 29-38

Lee CM; Kang KH; Cho NS (1998) Prediction of oil-droplet motion and containment of spilt oil with tandem oil fences. Proc. of 4th KSME-JSME Fluids Eng. Conf., Haeundae, Pusan, Oct 18-21, 465-468

Lo JM, (1996) Laboratory investigation of single floating booms and series of booms in the prevention of oil slick and jellyfish movement. Ocean Engineering, 23: 519-531

Song MS; Hyun BS; Suh JC (1998) Containment failures of oil restricted vertical plates in current. J. of Korean Soc. for Marine Environmental Engineering, 1-2: 40-51

Utami T; Blackwelder R (1991) A cross correlation technique for velocity field extraction from particulate visualization. Exp. in Fluids, 10: 213-223